



HHS Public Access

Author manuscript

Clin Cancer Res. Author manuscript; available in PMC 2020 February 15.

Published in final edited form as:

Clin Cancer Res. 2019 February 15; 25(4): 1206–1215. doi:10.1158/1078-0432.CCR-18-2665.

Preclinical development and first-in-human imaging of the integrin $\alpha_v\beta_6$ with [^{18}F] $\alpha_v\beta_6$ -Binding Peptide in metastatic carcinoma.

Sven H. Hausner¹, Richard J. Bold², Lina Y. Cheuy³, Helen K. Chew¹, Megan E. Daly⁴, Ryan A. Davis¹, Cameron C. Foster⁵, Edward J. Kim¹, and Julie L. Sutcliffe^{1,3,6}

¹Division of Hematology/Oncology, Department of Internal, Medicine. University of California Davis, Davis and Sacramento, CA, USA

²Division of Surgical Oncology, Department of Surgery, University of California Davis, Davis and Sacramento, CA, USA

³Department of Biomedical Engineering, University of California Davis, Davis and Sacramento, CA, USA

⁴Department of Radiation Oncology, University of California Davis, Davis and Sacramento, CA, USA

⁵Division of Nuclear Medicine, Department of Radiology, University of California Davis, Davis and Sacramento, CA, USA

⁶Center for Molecular and Genomic Imaging., University of California Davis, Davis and Sacramento, CA, USA

Abstract

Purpose: The study was undertaken to develop and evaluate the potential of an integrin $\alpha_v\beta_6$ -binding peptide ($\alpha_v\beta_6$ -BP) for noninvasive imaging of a diverse range of malignancies with positron emission tomography (PET).

Experimental Design: The peptide $\alpha_v\beta_6$ -BP was prepared on solid phase and radiolabeled with 4- ^{18}F fluorobenzoic acid. *In vitro* testing included ELISA, serum stability, and cell binding studies using a paired $\alpha_v\beta_6$ -expressing and $\alpha_v\beta_6$ -null cell lines. *In vivo* evaluation (PET/CT,

Corresponding author: Julie Sutcliffe, Division of Hematology/Oncology, Department of Internal Medicine, 2921 Stockton Blvd, University of California Davis, Sacramento, CA 95817. Tel.: 916 734 5536; fax: 916 734 7572; jlsutcliffe@ucdavis.edu.

Authors' contributions

Conception and design: Sutcliffe J. L., Bold R. J., and Hausner S. H.

Development of methodology: Sutcliffe J. L., Bold R. J., Davis R. A., Hausner S. H., and Foster C. F.

Acquisition of data (provided animals, acquired and managed patients, provided facilities, etc.): Bold R. J., Cheuy L. Y., Chew H. K., Daly M. E., and Kim E. J.

Analysis and interpretation of data (e.g., statistical analysis, biostatistics, computational analysis): Sutcliffe J. L., Bold R. J., Hausner S. H., and Foster C. F.

Writing, review, and/or revision of the manuscript: Sutcliffe J. L., Bold R. J., Cheuy L. Y., Chew H. K., Daly M. E., Davis R. A., Foster C. F., Hausner S. H and Kim E. J.

Study supervision: Sutcliffe J. L.

Conflict of Interest:

Sven Hausner and Julie Sutcliffe are named inventors of intellectual property related to [^{18}F] $\alpha_v\beta_6$ -BP. Julie Sutcliffe is the founder and stock holder of Luminance Biosciences, Inc.

biodistribution and autoradiography) was performed in a mouse model bearing the same paired $\alpha_v\beta_6$ -expressing and $\alpha_v\beta_6$ -null cell xenografts. A first-in-human PET/CT imaging study was performed in patients with metastatic lung, colon, breast or pancreatic cancer.

Results: [^{18}F] $\alpha_v\beta_6$ -BP displayed excellent affinity and selectivity for the integrin *in vitro* ($\text{IC}_{50}(\alpha_v\beta_6) = 1.2 \text{ nM}$ vs $\text{IC}_{50}(\alpha_\beta_3) > 10 \mu\text{M}$) in addition to rapid target-specific cell binding and internalization ($72.5 \pm 0.9\%$ binding and $52.5 \pm 1.8\%$ respectively). Favorable tumor affinity and selectivity were retained in the mouse model and excretion of unbound [^{18}F] $\alpha_v\beta_6$ -BP was rapid, primarily via the kidneys. In patients, [^{18}F] $\alpha_v\beta_6$ -BP was well tolerated without noticeable adverse side effects. PET images showed significant uptake of [^{18}F] $\alpha_v\beta_6$ -BP in both the primary lesion and metastases, including metastasis to brain, bone, liver and lung.

Conclusions: The clinical impact of [^{18}F] $\alpha_v\beta_6$ -BP PET imaging demonstrated in this first-in-human study is immediate for a broad spectrum of malignancies.

Keywords

Integrin $\alpha_v\beta_6$; Positron Emission Tomography; first-in-human; peptide; metastases

Introduction

A central tenet for the delivery of personalized therapy in the treatment of cancer patients is the accurate evaluation of the extent of disease, which has primarily relied on a variety of radiologic studies [1, 2]. [^{18}F]FDG-PET/CT allows whole body imaging and has been incorporated into clinical practice for both initial evaluation of disease sites as well as a surrogate for response to therapy. Yet significant limitations exist for [^{18}F]FDG-PET/CT including the lack of a target that is specific and biologically relevant to cancer cells [2–5]. There is a significant and rapidly growing body of literature that has identified the integrin $\alpha_v\beta_6$ as one such target. This integrin is an epithelial-specific cell surface receptor that is usually undetectable in healthy adult epithelium but is significantly up-regulated in a wide range of epithelial-derived cancers including breast, colon, non-small cell lung, oral squamous cell carcinoma, ovarian and pancreas cancer [6–15]. Furthermore, higher levels of expression have been correlated with invasiveness and clinically this has been correlated with metastatic progression and poor patient survival [10, 14–20]. The preferential expression of this integrin in neoplastic tissues as well as the scope of malignancies over-expressing this integrin suggests that agents specifically targeting $\alpha_v\beta_6$ have significant potential in the evaluation, treatment, and management of multiple types of solid organ malignancies. Given the impact of molecular imaging in oncology, our group and others have chosen to develop $\alpha_v\beta_6$ specific PET molecular imaging agents [21–23].

The prototypical structure of $\alpha_v\beta_6$ integrin binding agents has been based on the RG/TDLXXL motif [24] and these agents have undergone extensive preclinical evaluation. Several molecular imaging agents, including those identified using phage display [8] and cysteine knottin peptides [25], have been investigated. Our efforts have focused primarily on the 20-amino acid peptide A20FMDV2 that was first identified from the GH-loop of the VP1 protein of foot and mouth disease virus, which uses the $\alpha_v\beta_6$ integrin to mediate host cell infection [23]. Building upon the information obtained using our first generation

peptide, [^{18}F]FBA-A20FMDV2, and through subsequent structure-activity studies, derivatization through the addition of PEG modifiers, and *in vitro* and *in vivo* mouse studies, we developed [^{18}F] $\alpha_v\beta_6$ -BP.

Herein we present the development of our lead candidate [^{18}F] $\alpha_v\beta_6$ -BP, including the *in vitro* testing, *in vivo* evaluation in mouse xenograft models of human cancer, and ultimately the first-in-human PET imaging in patients with a diagnosis of breast, colon, lung, or pancreas cancer. The data demonstrate the potential for molecular imaging of a broad spectrum of malignancies using [^{18}F] $\alpha_v\beta_6$ -BP.

Materials and Methods

General.

The general reagents and consumables for the synthesis of the peptides used in the preclinical and clinical studies, and the HPLC and analytical methods used, are described in the Supplementary Data.

Preclinical studies: Chemistry, radiochemistry, *in vitro*, and *in vivo* studies

Chemistry and radiochemistry.—Peptide synthesis and radiolabeling were performed on solid support and the radiotracer formulated in serum-free DMEM (for *in vitro* studies) or PBS (for *in vivo* studies) [26]. The cold standard [^{19}F] $\alpha_v\beta_6$ -BP was prepared by coupling 4-fluorobenzoic acid, pre-activated with 1-[bis(dimethylamino)methylene]-1*H*-1,2,3-triazolo[4,5-*b*]pyridinium 3-oxid hexafluorophosphate (HATU) and *N,N*-diisopropylethylamine (DIPEA), to the H_2N -peptidyl-resin; cleavage, purification, analysis and storage followed procedures described previously [27, 28]. Radiosynthesis of [^{18}F] $\alpha_v\beta_6$ -BP on solid support was done by coupling 4- [^{18}F]fluorobenzoic acid (FBA) [29], pre-activated with HATU and DIPEA, to 5 mg of pre-swollen H_2N -peptidyl-resin in a 1-mL fritted syringe reactor; following cleavage with trifluoroacetic acid (TFA)/water/triisopropylsilane (TIPS) 95/2.5/2.5 (v/v/v; 2 \times 0.5 mL; 15 min/each), [^{18}F] $\alpha_v\beta_6$ -BP was purified by high performance liquid chromatography (HPLC) and formulated [27].

In vitro evaluation

ELISA.—Competitive binding enzyme-linked immunosorbent assays (ELISAs) for integrins $\alpha_v\beta_6$ and $\alpha_v\beta_3$ were performed with [^{19}F] $\alpha_v\beta_6$ -BP as previously described and analyzed using Prism software (GraphPad Software, La Jolla, CA) [23].

Cell binding.—The cell lines DX3puro β_6 ($\alpha_v\beta_6$ positive) and DX3puro ($\alpha_v\beta_6$ negative) were cultured at 37° C under 5% CO_2 in DMEM containing 10% heat-inactivated FBS and 1% PSG [26, 27]. Expression levels of $\alpha_v\beta_6$ were confirmed by flow cytometry prior to the experiment. Binding of [^{18}F] $\alpha_v\beta_6$ -BP to and internalization into DX3puro β_6 and DX3puro cells were determined as previously described [26, 27]. Cell-binding samples were counted on a Wizard 1470 γ -counter (PerkinElmer, Waltham, MA).

Serum stability.—To evaluate serum-stability, mouse serum (Sigma Aldrich) was combined with the [^{18}F] $\alpha_v\beta_6$ -BP, incubated at 37° C for various amounts of time, and,

following precipitation of serum proteins with ethanol, analyzed by HPLC as previously described [26].

In vivo studies in mice.—All animal procedures conformed to the Animal Welfare Act and were approved by the university's Institutional Animal Care and Use Committee. Female athymic nude mice (Charles River Laboratories; Wilmington, MA) were inoculated subcutaneously with 3×10^6 DX3puro and 3×10^6 DX3puro β_6 cells on opposite flanks. Studies commenced once tumors reached a maximum diameter of ~ 0.5 cm (range 43–225 mg).

The [^{18}F] $\alpha_v\beta_6$ -BP was injected into the tail vein of mice (imaging: 9.0–9.5 MBq/animal; biodistribution: 1.5–2.0 MBq/animal; autoradiography: 37 MBq/animal). For imaging, two mice/scan were placed side-by-side in a feet-first, prone position ($n = 4$ total; anesthesia: 1.5–2.0% isoflurane); PET/CT scans (dynamic 4×15 -min PET emission scan starting 15 min post injection [p.i.], single-frame 15-min PET emission scans at 2 and 4 h p.i.) were acquired using Inveon scanners (Inveon DPET scanner and Inveon SPECT/CT scanner, Siemens Medical Solutions, Knoxville, TN) and analyzed as previously described using Inveon Research Workplace software (Siemens)[26].

For biodistribution studies, mice were euthanized and dissected 1, 2, and 4 hours ($n=3$ /time point) following injection of [^{18}F] $\alpha_v\beta_6$ -BP; blocking studies were conducted by pre-administration with [^{19}F]FBA-PEG₂₈-A20FMDV2 [30 mg/kg, 10 mg/mL in saline, intravenously [IV] ten minutes before the [^{18}F] $\alpha_v\beta_6$ -BP [30]. Tissues were collected, rinsed, and radioactivity measured in a γ -counter; calibrated, decay-corrected radioactivity concentrations are expressed as percent of injected dose per gram of sample (% ID/g). For autoradiography of [^{18}F] $\alpha_v\beta_6$ -BP tumor uptake and correlation to integrin $\alpha_v\beta_6$ -expression by immunohistochemistry (IHC), one animal was injected with [^{18}F] $\alpha_v\beta_6$ -BP and tumor tissue collected (1 h p.i.), embedded in freezing medium (Tissue-Tek, Sakura, Torrance, CA), and sectioned (CM 1850 cryostat, Leica Biosystems, Wetzlar, Germany). Autoradiography sections (20 μm) were exposed to a storage phosphor-screen overnight and the screen read on a STORM 860 phosphor imager at 50 μm resolution (GE Healthcare, Chicago, IL). For integrin $\alpha_v\beta_6$ IHC, adjacent sections (5 μm) were cut and fixed for staining [26].

Immunohistochemistry.—IHC sections were stained using anti-integrin β_6 antibody (Calbiochem Clone 442.5C4, 1:200 dilution) on a DAKO link autostainer (Agilent, Santa Clara, CA). The same method was used for assessment of β_6 expression of human samples.

Statistical analysis

Quantitative data are reported as mean \pm standard deviation (SD). Statistical analysis was done using a paired two-tailed Student's *t*-tests to evaluate statistical significance, where $P < 0.05$ was considered statistically significant.

First-in-human clinical study: Chemistry, radiochemistry, quality assurance, animal toxicity study GLP synthesis of precursor peptide, animal toxicity study.

The GLP synthesis of the precursor peptide H₂N- $\alpha_v\beta_6$ -BP, and single dose acute toxicity study of the [¹⁹F] $\alpha_v\beta_6$ -BP are described in the Supplementary Methods.

[¹⁸F] $\alpha_v\beta_6$ -BP synthesis, purification and quality assurance for human use.

[¹⁸F] $\alpha_v\beta_6$ -BP was manufactured in compliance with current good manufacturing practice (cGMP) under the guidelines of USP Chapter <823> for administration to human subjects as a single intravenous dose under the auspices of a FDA-approved exploratory investigational new drug (eIND #124336).

[¹⁸F]SFB synthesis and purification.

The *N*-succinimidyl 4-[¹⁸F]fluorobenzoate ([¹⁸F]SFB) was prepared on the GE TracerLab FX-FN one-pot automated synthesizer (GE Healthcare, Waukesha, WI) from azeotropically dried [¹⁸F]fluoride in Kryptofix (10 mg/mL)/potassium carbonate (2 mg/mL) solution (acetonitrile/water 94/6 v/v) and 4-(ethoxycarbonyl)-*N,N,N*-trimethylbenzenaminium triflate (5 mg; 90° C, 10 min, acetonitrile), followed by saponification with tetrapropylammonium hydroxide (20 μ L of 25% aq solution; 120° C, 1 min, acetonitrile) and subsequent activation using *O*-(*N*-succinimidyl-*N,N,N',N'*-tetramethyluronium tetrafluoroborate (TSTU) (12 mg; 90° C, 5 min, acetonitrile) to yield [¹⁸F]SFB. The crude [¹⁸F]SFB was purified by HPLC (Jupiter Proteo 10 μ m 90 Å column, 250 \times 10 mm; isocratic 10 mM phosphoric acid/acetonitrile 67/33 v/v, 5 mL/min). The HPLC fraction containing the [¹⁸F]SFB was trapped on a Sep-Pak C18 Plus cartridge, washed with water (5 mL), eluted with acetonitrile (1.5 mL) and dried by passing over a Sep-Pak Dry Sodium Sulfate Plus cartridge.

[¹⁸F] $\alpha_v\beta_6$ -BP synthesis and purification.

Following evaporation of the solvent (50° C, 10 min), the [¹⁸F]SFB was reconstituted with dimethylsulfoxide (DMSO, 245 μ L) containing the precursor peptide H₂N- $\alpha_v\beta_6$ -BP (0.5 mg) and DIPEA (5 μ L). The coupling reaction was allowed to proceed for 30 min (15 min at ambient temperature, followed by 15 min at 50° C), quenched with phosphoric acid (10 mM, 0.75 mL), and purified by semi-preparative HPLC. The fraction containing pure [¹⁸F] $\alpha_v\beta_6$ -BP was collected (3 mL) through a sterile 0.22 μ m filter (SLGVM33RS; MilliporeSigma), formulated by dilution with saline (to a final volume of 20 mL) and dispensed through a sterile 0.22 μ m filter (SLGVM33RS; MilliporeSigma) to yield [¹⁸F] $\alpha_v\beta_6$ -BP in a 10% ethanolic v/v solution in saline.

[¹⁸F] $\alpha_v\beta_6$ -BP quality assurance.

Prior to injection, quality testing including visual clarity, filter integrity, pH, radionuclidic identity, purity and radiochemical identity via analytical HPLC, residual solvent analysis via gas chromatography (GC), residual Kryptofix spot test and pyrogenicity via limulus amoebocyte lysate (LAL) test (Charles River Laboratories) were performed. The full list of release criteria is given in Supplemental Table S1 in the Supplementary Data; they also included a post-release 14-day sterility test using the direct inoculation of media method described in USP <71>.

First-in-human clinical study with [¹⁸F]α_vβ₆-BP: IRB approval and patient consent

This study protocol was approved by the UC Davis Institutional Review Board (FWA00004557) and written informed consent was obtained from all individual participants included in the study (Clinical Trials.gov NCT03164486). All subjects enrolled to this study signed a consent form that provided their consent for the testing of the [¹⁸F]α_vβ₆-BP and the analysis of biopsy material for research purposes. The inclusion and exclusion criteria for the study are provided in the Supplementary Data. The studies were conducted following U.S. Common Rule.

First-in-human clinical study: Data acquisition and data analysis Scanning protocol for PET/CT acquisition and image analysis.

Imaging was performed on a General Electric 690 time-of-flight PET scanner fitted with a 16-slice CT. Up to 370 MBq (326±44 MBq, in up to 10 mL) of [¹⁸F]α_vβ₆-BP were injected [IV] over 1 minute. Immediately after the injection vital signs (heart rate, pulse oximetry value, body temperature, EKG) were measured. Patients underwent PET/CT scanning from the apex of the skull to the proximal thighs with arms raised, using two minutes per bed position starting at 30 minutes, 1 hour, 2 hours and 3 hours post injection.

Data were reconstructed using the Ordered Subsets – Expectation Maximization (OSEM) algorithm, with 24 subsets and 2 iterations, and reviewed in the axial, coronal and sagittal planes. A 6.4 mm filter was used transaxially and the manufacturer’s “standard” filter was used axially. Image review was performed using GE Advantage Workstation software version 4.5. SUV_{max} values were obtained for lesions using manual sizing of rectangular ROI and standard 42% threshold.

Adverse Event monitoring.

Vital signs were checked at 15, 30, 45, 60, 75, 90, 105, 120, 135, 150, 165 and 180 min. In addition, vital signs and blood samples were obtained and checked 1 and 7 days after injection of [¹⁸F]α_vβ₆-BP to ensure no changes or abnormalities occurred. Pre-injection and follow-up blood draws were assessed for complete metabolic panel including liver function tests.

Serum stability and clearance of [¹⁸F]α_vβ₆-BP in humans.

Blood samples (1 mL) were taken throughout the imaging period (1, 3, 5, 10, 15, 30, 60, 90, 120, 180 min), collected in heparinized tubes, and immediately stored on ice and processed.

Stability: The 30 min blood sample was centrifuged (1130 × g, 10 min; 4° C), proteins precipitated from the supernatant with an equal volume of ethanol and removed by centrifugation (11,160 × g, 3 min; 4° C). The protein removal process was repeated with a half-volume of ethanol. The final supernatant was diluted with an equal volume water/TFA (0.05% v/v)/glacial acetic acid (2% v/v) for HPLC analysis.

Clearance: At each collection time point, a whole-blood aliquot (200 μL) was transferred to a γ-counter tube; cells were precipitated in the remaining sample by centrifugation (1130 × g, 10 min; 4° C) and a plasma aliquot (200 μL) was transferred to a γ-counter tube.

Samples were counted on a γ -counter and radioactivity concentrations calculated as decay-corrected percent of injected dose per gram of sample [dc % ID/g].

Results

Chemistry and radiochemistry

Non-radioactive [^{19}F] $\alpha_v\beta_6$ -BP was obtained in >98% purity after HPLC purification; [^{19}F] $\alpha_v\beta_6$ -BP: MS (MALDI) $m/z = 4919.9564$ [$\text{M}+\text{H}$] $^+$, calculated M (FBA-PEGNAVPNLRGDLQVLAQRVARTPEG; $\text{C}_{218}\text{H}_{401}\text{FN}_{36}\text{O}_{86}$) = 4918.8096, 4919.8174 [$\text{M}+\text{H}$] $^+$. For preclinical studies, the radiotracer [^{18}F] $\alpha_v\beta_6$ -BP was prepared by solid-phase radiolabeling with [^{18}F]FBA and obtained in 98.1 \pm 1.0% radiochemical purity with a molar activity of 65 \pm 25 GBq/ μmol and a decay-corrected radiochemical yield of 6.6 \pm 1.0% from [^{18}F]FBA ($n = 10$). For clinical production [^{18}F] $\alpha_v\beta_6$ -BP was prepared in solution with [^{18}F]SFB in radiochemical purity 99% with molar activity 37 GBq/ μmol , mass dose 50 μg /patient dose, and 15.1 \pm 1.7% decay-corrected radiochemical yield from [^{18}F]SFB ($n = 18$).

Preclinical *in vitro* studies

In vitro affinity and selectivity were evaluated by competitive ELISA against the biotinylated natural ligands and by cell-binding studies using the integrin $\alpha_v\beta_6$ -expressing cell line DX3puro β_6 and the paired non- $\alpha_v\beta_6$ -expressing DX3puro control; affinity (IC_{50}) of [^{19}F] $\alpha_v\beta_6$ -BP for integrin $\alpha_v\beta_6$ was 1.2 nM, whereas no binding was observed to integrin $\alpha_v\beta_3$ at concentrations up to 10 μM (Fig. 1 A). Cell binding studies with [^{18}F] $\alpha_v\beta_6$ -BP resulted in 72.5 \pm 0.9% of total radioactivity bound to DX3puro β_6 cells at 1 h, with 52.5 \pm 1.8% of total radioactivity internalized (corresponding to 72.4 \pm 2.5% of bound radioactivity; Fig. 1 B); binding to and internalization in DX3puro cells was 3.5 \pm 1.4% and 1.0 \pm 0.1% of total radioactivity, respectively. Therefore the ratios of $\alpha_v\beta_6$ -expressing cell line compared to the non-expressing cell line (DX3puro β_6 /DX3puro) were 21/1 and 54/1, respectively, for total bound and internalized radioactivity ($P = 2 \times 10^{-10}$, $P = 1 \times 10^{-8}$). In mouse serum, [^{18}F] $\alpha_v\beta_6$ -BP remained 98.3% intact at 30 min at 37 $^{\circ}\text{C}$; with minimal metabolism at 60 and 120 minutes (93.3% and 88.9% intact, respectively).

Preclinical *in vivo* studies

Evaluation of [^{18}F] $\alpha_v\beta_6$ -BP in the paired DX3puro β_6 /DX3puro tumor mouse model showed DX3puro β_6 -tumor uptake of 2.51 \pm 0.48% ID/g at 1 h and good retention (2.64 \pm 1.23% ID/g at 4 h), while uptake and retention in the $\alpha_v\beta_6$ -negative DX3puro control tumor were low (1 h: 0.35 \pm 0.14% ID/g; 4 h: 0.21 \pm 0.15% ID/g; Supplemental Table S2). This resulted in a steady increase in DX3puro β_6 -to-DX3puro tumor ratio from 8.3 \pm 4.2/1 at 1 h to 18.3 \pm 11.7/1 at 4 h (Supplemental Table S2). When $\alpha_v\beta_6$ -blocking peptide was pre-administered ten minutes before the radiotracer, DX3puro β_6 tumor uptake was reduced by 90% to 0.28 \pm 0.07% ID/g (1 h; $P = 0.001$), a level comparable to uptake in the DX3puro control tumor (0.26 \pm 0.03% ID/g).

IHC staining for integrin $\alpha_v\beta_6$ confirmed expression in DX3puro β_6 tumors, and the distribution of integrin $\alpha_v\beta_6$ corresponded to the distribution of [^{18}F] $\alpha_v\beta_6$ -BP as determined

by autoradiography. By comparison, both staining for integrin $\alpha_v\beta_6$ and uptake of [^{18}F] $\alpha_v\beta_6$ -BP were at background levels for the DX3puro control tumors (Fig. 1 D).

PET/CT imaging correlated with the biodistribution data, clearly visualizing the DX3puro β_6 tumor while showing no uptake in the DX3puro tumor (Fig. 1 C). Imaging and biodistribution demonstrated rapid renal clearance as the major route of elimination, with minor hepatobiliary contribution (Fig. 1 and Supplemental Table S2). Highest uptake was seen for kidneys at 1 h ($22.9\pm 8.9\%$ ID/g), rapidly clearing to $7.9\pm 2.1\%$ ID/g at 4 h; all other organs showed $<8\%$ ID/g at 1 h and $<6\%$ ID/g at 4 h, with stomach, gallbladder, lung, and bladder being 5.6 ± 1.6 , 4.5 ± 3.0 , 2.3 ± 0.2 , and $1.8\pm 1.8\%$ ID/g, respectively, at 4 h (Supplemental Table S2).

First-in-human clinical study with [^{18}F] $\alpha_v\beta_6$ -BP

Patients with a prior diagnosis of breast, colon, lung or pancreas cancer were recruited to the study (18 patients to date). The mean injected dose of [^{18}F] $\alpha_v\beta_6$ -BP was 326 ± 44 MBq (range: 220–364 MBq) with a mass dose 50 μg /patient dose. No noticeable changes in vital signs, on electrocardiograms, or in blood laboratory results were observed during the study, and no adverse side effects were noted at the 7 day follow-up after injection of the radiotracer.

Stability of [^{18}F] $\alpha_v\beta_6$ -BP in human blood, blood clearance, and general biodistribution:

[^{18}F] $\alpha_v\beta_6$ -BP was rapidly cleared from the blood stream (Supplemental Fig. S1); radio-HPLC of blood samples taken 30 minutes after injection showed no metabolite peaks and indicated that [^{18}F] $\alpha_v\beta_6$ -BP remained intact (Supplemental Fig. S2). PET images demonstrated significant uptake of [^{18}F] $\alpha_v\beta_6$ -BP in the primary and metastatic lesions, including sub-centimeter lesions in adrenal glands, bone, brain, liver and lung (Figures 2–6 and Supplemental Table S4). For example, for subject #1 the primary tumor to background ratio was 17.3:1 and right Iliac wing lesion to background ratio was 67.5:1. For subject #2 the primary tumor to background ratio was 19.5:1 and the left Iliac bone lesion to background ratio was 43.7:1. Concordant with the murine data, rapid renal excretion of [^{18}F] $\alpha_v\beta_6$ -BP was observed with minimal uptake in normal bone, brain liver or lung (i.e. major sites of metastasis). Evaluation of specific tissues demonstrated low to mild activity in the pituitary, lacrimal and salivary glands where it decreased during the imaging timeframe, and in the thyroid where it appeared stable (Supplemental Table S3). High uptake was seen in the kidneys and was stable over the imaging timeframe whereas the bladder demonstrated low to moderate and variable activity depending on fluid and voiding status. The average radioactivity uptake in the entire stomach was moderate and steady throughout the imaging timeframe, however uptake observed in the fundus overall minimally decreased over time. The average radioactivity uptake in the entire small bowel was moderate and increased over time. The ascending and descending colon demonstrated overall mild to moderate activity that increased over time to moderate activity. Initial impression of bowel activity and distribution pattern suggests uptake and secretion from the stomach and anterograde movement of activity over time in the bowel lumen. A summary of the SUV_{max} data at the 1 h and 3 h time points for the five patients presented here is listed in the Supplemental Table S3.

Representative individual observations.

Subject 1 was a 53 year old female diagnosed with stage IV adenocarcinoma of the lung. Uptake of [^{18}F] $\alpha_v\beta_6$ -BP was observed in both the primary lung lesion and a right iliac wing bone metastasis (Fig. 2 A and Fig. 2 B). At the 1 h scan, a SUV_{max} of 5.2 and 13.5 was observed for the primary lung lesion and right iliac wing metastasis respectively (Fig. 2 and Supplemental Table S4). Analysis of a sample of a malignant pleural effusion demonstrated strong expression of the integrin $\alpha_v\beta_6$ (Fig. 2 C a-b).

Subject 2 was a 59 year old female diagnosed with stage IV invasive mammary carcinoma. Uptake of [^{18}F] $\alpha_v\beta_6$ -BP was observed in the primary breast lesion as well as in metastases in multiple lymph nodes in the right axilla and mediastinum, and multiple osseous sites. At the 1 h scan, a SUV_{max} of 3.9 was observed in the primary lesion and SUV_{max} ranged from 4.4–13.1 in the lymph nodes and metastases (Fig. 3 and Supplemental Table S4). Tissue from the primary lesion and the left iliac osseous metastasis were available and demonstrated high levels of $\alpha_v\beta_6$ expression (Fig. 3 C a-d).

Subject 3 was a 56 year old female diagnosed with initial stage IIIB adenocarcinoma of the lung, subsequently metastatic. Uptake of [^{18}F] $\alpha_v\beta_6$ -BP was observed in the primary lung lesion in addition to multiple sites of metastases including brain, right adrenal gland, perifacial lymph node and osseous sites. At the 1 h scan, a SUV_{max} of 10.6 was observed in the consolidated mass in the lung and the SUV_{max} ranged from 1.0–7.3 in the lymph node, right adrenal and osseous metastasis (Supplemental Tables S3 and S4). The [^{18}F] $\alpha_v\beta_6$ -BP PET images revealed numerous brain metastases, in the right and left parietal, left frontal and occipital lobes, with SUV_{max} of 2.7, 2.4, 2.4, and 1.0, respectively. Representative axial images are shown in Fig. 4, middle row); all regions demonstrating increased SUV_{max} , were clearly visualized against a brain background SUV_{max} of 0.1, and correlated with the known brain metastases visualized on MRI (Fig. 4, upper row).

Subject 4 was a 51 year old female diagnosed with initial stage IV adenocarcinoma of the colon with metastases to liver, lungs and abdominal lymph nodes at time of diagnosis. Uptake of [^{18}F] $\alpha_v\beta_6$ -BP was observed in two sites in the left lobe of the liver (Fig. 5), bilateral lobes of the lungs and lymph nodes of the thorax / low neck. At the 1 h scan, a SUV_{max} of 2.3 was observed in an upper left hepatic lobe lesion (Fig. 5 and Supplemental Table S4), 3.4 in a lower lateral left hepatic lobe lesion, a range of 0.6–0.9 for the right and left pulmonary lesions and a range of 1.4–1.7 for the thoracic and low neck lymph nodes (Supplemental Table S4)

Subject 5 was a 78 year old male diagnosed with initial stage IV adenocarcinoma of the pancreas with metastases to the lung at time of diagnosis. Uptake of [^{18}F] $\alpha_v\beta_6$ -BP was observed in multiple small right lower lobe pulmonary densities (example depicted in Fig. 6). At the 1 h scan, a SUV_{max} range of 0.6–1.4 (Supplemental Table S4) was seen in the pulmonary densities ranging in size from 0.6–0.8 cm.

Discussion

There is increasing evidence of the important role of integrin $\alpha_v\beta_6$ in cancer, its suitability as a prognostic biomarker (linked to poor disease-free and overall survival) and the promise

of an $\alpha_v\beta_6$ -targeted clinical diagnostic tool for *in vivo* detection patient stratification, as well as monitoring of response to treatment [31–33]. The high contrast in signal gained due to aberrant, but specific expression of $\alpha_v\beta_6$ suggests that $\alpha_v\beta_6$ -targeted agents have significant potential in the treatment and management of a multitude of malignancies. This has led to the development of several pre-clinical PET and single photon emission computed tomography (SPECT) radiotracers and, most recently, clinical reports in patients with head and neck squamous cell carcinoma (HNSCC) and NSCLC [34].

The integrin $\alpha_v\beta_6$ is a receptor for fibronectin, tenascin, vitronectin, the latency associated peptide (LAP) of the transforming growth factor-beta (TGF β) and the VP1 coat protein of foot and mouth disease virus (FMDV). Our first generation $\alpha_v\beta_6$ -targeting peptide was A20FMDV2, a 20 amino acid peptide (NAVPNLRGDLQVLAQKVART), from the sequence of the GH-loop of the VP1 protein from FMDV [35, 36]. We initially demonstrated the promise of A20FMDV2 as an *in vivo* imaging agent for $\alpha_v\beta_6$ with the 4- ^{18}F fluorobenzoyl labeled ^{18}F FBA-A20FMDV2 [23]. Although $\alpha_v\beta_6$ -specific targeting *in vivo* was observed in murine xenograft models, rapid tumor wash out (0.66% ID/g at 1 h, down to 0.06% ID/g at 4 h) and poor *in vivo* stability precluded its further application. This motivated us to investigate a series of improvements (mainly through the size and locations of PEG modifiers and subsequent confirmation by structure-activity studies), culminating in ^{18}F $\alpha_v\beta_6$ -BP as the lead compound for translation to a human clinical trial.

In vitro affinity and selectivity of ^{18}F $\alpha_v\beta_6$ -BP for integrin $\alpha_v\beta_6$ were excellent and compared favorably to those reported by Altmann et al. for their SFTI-1 derivatives, however it is noted that the experimental methods were somewhat different, and different cells lines with varying expression levels of the integrin $\alpha_v\beta_6$ were used [37]. *In vivo* studies using the paired DX3puro β_6 /DX3puro cell xenograft mouse model confirmed that ^{18}F $\alpha_v\beta_6$ -BP met expectations for $\alpha_v\beta_6$ targeting and overall pharmacokinetics, with good tumor retention and kidney clearance. The tumor uptake values were similar to those noted by Altmann et al. for their SFITGv6 peptide which demonstrated good binding in mice bearing HNO97 xenografts [37].

Given these favorable *in vitro* and *in vivo* results of ^{18}F $\alpha_v\beta_6$ -BP, we proceeded with our first-in-human microdose study to evaluate the safety and *in vivo* behavior of ^{18}F $\alpha_v\beta_6$ -BP (exploratory Investigational New Drug [eIND] # 124336, NCT03164486). The evaluation of the overall pharmacokinetics revealed- that ^{18}F $\alpha_v\beta_6$ -BP was predominantly excreted renally, with moderate transient activity in the gastrointestinal tract and mild activity in the pituitary, lacrimal, salivary glands and the thyroid. Minimal uptake was found in the four common sites of metastatic disease, namely bone, brain, liver and lung.

Our observations align closely with those described by Keat et al. who recently reported a microdose study in four healthy subjects using our first generation compound ^{18}F FBA-A20FMDV2 [38]. Similar uptake in the thyroid, salivary glands, kidney and stomach was noted; however, they also observed additional significant uptake in the gallbladder, liver, and spleen. The lack of uptake of ^{18}F $\alpha_v\beta_6$ -BP in these organs is due to the peptide modifications introduced; this improvement on biodistribution does provide lower background uptake and thus increases sensitivity for the detection of disease, as the liver is a

frequent site of metastases. Recently, Altmann et al. reported the results of PET/CT scans performed in a compassionate use setting in two patients with [^{68}Ga]-DOTA-SFITGv6, a SFTI-1 derived peptide targeting $\alpha_v\beta_6$ which was identified using phage display [37]. They describe a general biodistribution of their gallium-68 tracer similar to that of [^{18}F] $\alpha_v\beta_6$ -BP, revealing accumulation in the kidneys, with gastrointestinal secretion followed by an intraluminal transport to the terminal ileum and cecum. They concluded that these challenges could be overcome by the use of diuretics and laxatives respectively.

Although [^{18}F]FDG-PET/CT plays a crucial role in the staging of patients with a wide range of malignancies, its well-known limitations include uptake in inflamed or infected tissues and poor signal-to-noise ratio in the brain and liver [1, 2, 4, 5]. This limits the detection of primary and metastatic disease in these organs and highlights the need for cancer specific imaging agents such as [^{18}F] $\alpha_v\beta_6$ -BP. The integrin $\alpha_v\beta_6$ is often localized to the invasive front and infiltrating edges of tumors, plays a key role in invasion and metastases, and has been closely correlated with distant metastasis in breast, lung and colon cancer as well as lymph node metastasis in pancreas cancer [31]. Notably, the low non-specific uptake of [^{18}F] $\alpha_v\beta_6$ -BP in normal bone, brain, liver, and lung suggest [^{18}F] $\alpha_v\beta_6$ -BP as a promising imaging agent to detect metastases. Uptake of [^{18}F] $\alpha_v\beta_6$ -BP was observed in several sub-centimeter metastases in the lung of a patient with metastatic pancreatic adenocarcinoma (subject 5). This observation begins to address the issue of size threshold for detection of disease. In this respect, our data for [^{18}F] $\alpha_v\beta_6$ -BP indicate a very favorable performance characteristic for identification of small lesions that may be indeterminate on traditional thoracic CT imaging. The fact that pancreas cancer is one of the most lethal cancer in the USA, that the majority of patients present with metastatic disease at the time of presentation, and that detection of metastases markedly alters treatment amplifies the need for accurate non-invasive imaging [39]. Our preliminary data strongly demonstrate that [^{18}F] $\alpha_v\beta_6$ -BP holds tremendous promise to meet this need for accurate determination of the extent of disease.

This was further seen in the patient with stage IV invasive mammary carcinoma (subject 2) where uptake of [^{18}F] $\alpha_v\beta_6$ -BP was observed in the primary breast lesion as well as metastases in multiple lymph nodes. The uptake in the primary lesion and the left iliac osseous metastasis was subsequently confirmed by IHC to correlate with $\alpha_v\beta_6$ expression. Numerous reports have demonstrated that tumors originating from the breast express high levels of $\alpha_v\beta_6$ and suggests that there may be potential for broad utility in staging of breast cancer. Here, [^{18}F] $\alpha_v\beta_6$ -BP also demonstrated great promise to guide the staging and treatment of these patients as the identification of occult metastatic disease significantly alters the intent of therapy.

In subject 3 [^{18}F] $\alpha_v\beta_6$ -BP clearly identified known brain metastases as small as 0.5 cm with low background uptake in the brain parenchyma. These images demonstrated that [^{18}F] $\alpha_v\beta_6$ -BP enters the brain, targets metastases, and suggest that this radiotracer could provide combined staging of the brain and body within a single imaging study. To our knowledge, this case is the first to demonstrate PET imaging of brain metastases using an $\alpha_v\beta_6$ targeting peptide and suggests an exciting opportunity for high-resolution systemic staging and patient selection for novel therapeutics using [^{18}F] $\alpha_v\beta_6$ -BP PET/CT.

In conclusion, [^{18}F] $\alpha_v\beta_6$ -BP demonstrated high affinity and selectivity for integrin $\alpha_v\beta_6$ *in vitro* and *in vivo*, along with significantly improved pharmacokinetics over previous generations. [^{18}F] $\alpha_v\beta_6$ -BP can be prepared reliably for clinical imaging and is well tolerated by patients. Significant uptake of [^{18}F] $\alpha_v\beta_6$ -BP in both the primary lesion and in metastases in a variety of cancers was observed, and uptake correlated with $\alpha_v\beta_6$ expression as shown by IHC for all available specimen samples. Although preliminary, these results are very promising, are in concurrence with the pre-clinical observations, and demonstrate the ability to successfully image lesions well under 1 cm. Furthermore, a variety of sites of metastases including lung, liver, bone and brain were imaged as a result of the favorable pharmacokinetics coupled with the low background affinity in these common sites of metastasis. The clinical impact of this first-in-human study is immediate for a broad spectrum of malignancies. This approach facilitates precision medicine, with $\alpha_v\beta_6$ -directed imaging allowing the early detection and monitoring of response to therapy, thus enabling prediction of outcome and optimized treatment regimes.

Supplementary Material

Refer to Web version on PubMed Central for supplementary material.

Acknowledgements.

The authors acknowledge the nuclear medicine staff Denise Caudle, Heather Hunt and Kristen McBride for taking care of the patients and performing the PET/CT imaging, Dr. Abimbola Olusanya for consenting patients enrolled in this study, Regina Gandour-Edwards for performing the IHC staining, Jennifer Fung, Charles Smith, and David Kukis of the Center for Molecular and Genomic Imaging as well as David Boucher for support of the preclinical studies. Last but not least we thank all of our patient volunteers for selflessly dedicating their time. This work was funded in part through Department of Energy DE-SC0008385, NIH R01CA211554-01 and UC Davis Research in Science and Engineering.

Financial support:

Department of Energy, Office of Science, award #DE-SC0008385 UC Davis Research Investment in Science and Engineering grant National Institute of Health, award #R01CA211554-01

References:

1. Choudhury P and Gupta M, Personalized & Precision Medicine in Cancer: A Theranostic Approach. *Curr Radiopharm*, 2017 10(3): p. 166–170. [PubMed: 28758574]
2. Mahajan A, et al., Bench to bedside molecular functional imaging in translational cancer medicine: to image or to imagine? *Clin Radiol*, 2015 70(10): p. 1060–82. [PubMed: 26187890]
3. Huo E, et al., The Role of PET/MR Imaging in Precision Medicine. *PET Clin*, 2017 12(4): p. 489–501. [PubMed: 28867118]
4. Tagliabue L and Del Sole A, Appropriate use of positron emission tomography with [(18)F]fluorodeoxyglucose for staging of oncology patients. *Eur J Intern Med*, 2014 25(1): p. 6–11. [PubMed: 23910561]
5. Salmon E, Bernard Ir C, and Hustinx R, Pitfalls and Limitations of PET/CT in Brain Imaging. *Semin Nucl Med*, 2015 45(6): p. 541–51. [PubMed: 26522395]
6. Bandyopadhyay A and Raghavan S, Defining the role of integrin alpha(v)beta(6) in cancer. *Curr Drug Targets*, 2009 10(7): p. 645–52. [PubMed: 19601768]
7. Ahmed N, et al., Overexpression of alpha(v)beta6 integrin in serous epithelial ovarian cancer regulates extracellular matrix degradation via the plasminogen activation cascade. *Carcinogenesis*, 2002 23(2): p. 237–44. [PubMed: 11872628]

8. Elayadi AN, et al., A peptide selected by biopanning identifies the integrin alphavbeta6 as a prognostic biomarker for nonsmall cell lung cancer. *Cancer Res*, 2007 67(12): p. 5889–95. [PubMed: 17575158]
9. Moore KM, et al., Therapeutic targeting of integrin alphavbeta6 in breast cancer. *J Natl Cancer Inst*, 2014 106(8): p. 1–14
10. Zhang ZY, et al., Integrin alphavbeta6 acts as a prognostic indicator in gastric carcinoma. *Clin Oncol (R Coll Radiol)*, 2008 20(1): p. 61–6. [PubMed: 17981018]
11. Hsiao JR, et al., Cyclic alphavbeta6-targeting peptide selected from biopanning with clinical potential for head and neck squamous cell carcinoma. *Head Neck*, 2010 32(2): p. 160–72. [PubMed: 19572290]
12. Bates RC, The alphaVbeta6 integrin as a novel molecular target for colorectal cancer. *Future Oncol*, 2005 1(6): p. 821–8. [PubMed: 16556062]
13. Bates RC and Mercurio AM, The epithelial-mesenchymal transition (EMT) and colorectal cancer progression. *Cancer Biol Ther*, 2005 4(4): p. 365–70. [PubMed: 15846061]
14. Berghoff AS, et al., alphavbeta3, alphavbeta5 and alphavbeta6 integrins in brain metastases of lung cancer. *Clin Exp Metastasis*, 2014 31(7): p. 841–51. [PubMed: 25150423]
15. Sipos B, et al., Immunohistochemical screening for beta6-integrin subunit expression in adenocarcinomas using a novel monoclonal antibody reveals strong up-regulation in pancreatic ductal adenocarcinomas in vivo and in vitro. *Histopathology*, 2004 45(3): p. 226–36. [PubMed: 15330800]
16. Thomas GJ, Nystrom ML, and Marshall JF, Alphavbeta6 integrin in wound healing and cancer of the oral cavity. *J Oral Pathol Med*, 2006 35(1): p. 1–10. [PubMed: 16393247]
17. Allen MD, et al., Altered microenvironment promotes progression of preinvasive breast cancer: myoepithelial expression of alphavbeta6 integrin in DCIS identifies high-risk patients and predicts recurrence. *Clin Cancer Res*, 2014 20(2): p. 344–57. [PubMed: 24150233]
18. Ramos DM, et al., Expression of integrin beta 6 enhances invasive behavior in oral squamous cell carcinoma. *Matrix Biol*, 2002 21(3): p. 297–307. [PubMed: 12009335]
19. Bates RC, Colorectal cancer progression: integrin alphavbeta6 and the epithelial-mesenchymal transition (EMT). *Cell Cycle*, 2005 4(10): p. 1350–2. [PubMed: 16123591]
20. Hazelbag S, et al., Overexpression of the alpha v beta 6 integrin in cervical squamous cell carcinoma is a prognostic factor for decreased survival. *J Pathol*, 2007 212(3): p. 316–24. [PubMed: 17503414]
21. Hackel BJ, et al., 18F-Fluorobenzoate-labeled cystine knot peptides for PET imaging of integrin alpha(v)beta(6). *J Nucl Med*, 2013 54(7): p. 1101–5. [PubMed: 23670900]
22. Li S, et al., Synthesis and characterization of a high-affinity alpha(v)beta(6)-specific ligand for in vitro and in vivo applications. *Molecular Cancer Therapeutics*, 2009 8(5): p. 1239–1249. [PubMed: 19435868]
23. Hausner SH, et al., Use of a peptide derived from foot-and-mouth disease virus for the noninvasive imaging of human cancer: Generation and evaluation of 4-[18F]fluorobenzoyl A20FMDV2 for in vivo imaging of integrin alpha(v)beta(6) expression with positron emission tomography. *Cancer Research*, 2007 67(16): p. 7833–7840. [PubMed: 17699789]
24. Kraft S, et al., Definition of an unexpected ligand recognition motif for alphav beta6 integrin. *J Biol Chem*, 1999 274(4): p. 1979–85. [PubMed: 9890954]
25. Kimura RH, et al., Pharmacokinetically stabilized cystine knot peptides that bind alpha-v-beta-6 integrin with single-digit nanomolar affinities for detection of pancreatic cancer. *Clin Cancer Res*, 2012 18(3): p. 839–49. [PubMed: 22173551]
26. Hausner SH, Bauer N, and Sutcliffe JL, In vitro and in vivo evaluation of the effects of aluminum [18F]fluoride radiolabeling on an integrin alpha(v)beta(6)-specific peptide. *Nucl Med Biol*, 2014 41(1): p. 43–50. [PubMed: 24267053]
27. Hausner SH, et al., Evaluation of [64Cu]Cu-DOTA and [64Cu]Cu-CB-TE2A chelates for targeted positron emission tomography with an alpha(v)beta(6)-specific peptide. *Molecular Imaging*, 2009 8(2): p. 111–121. [PubMed: 19397856]

28. Hausner SH, et al., The effect of bi-terminal PEGylation of an integrin alpha(v)beta(6)-targeted 18F peptide on pharmacokinetics and tumor uptake. *Journal of Nuclear Medicine*, 2015 56(5): p. 784–790. [PubMed: 25814519]
29. Davis RA, et al., Solid-phase synthesis and fluorine-18 radiolabeling of cycloRGDyK. *Org. Biomol. Chem*, 2016 14(37): p. 8659–8663. [PubMed: 27714190]
30. Hausner SH, et al., Targeted in vivo imaging of integrin alpha(v)beta(6) with an improved radiotracer and its relevance in a pancreatic tumor model. *Cancer Research*, 2009 69(14): p. 5843–5850. [PubMed: 19549907]
31. Niu J and Li Z, The roles of integrin alphavbeta6 in cancer. *Cancer Lett*, 2017 403: p. 128–137. [PubMed: 28634043]
32. Koivisto L, et al., Integrin alphavbeta6: Structure, function and role in health and disease. *Int J Biochem Cell Biol*, 2018 99: p. 186–196. [PubMed: 29678785]
33. Farber SF, et al., Therapeutic Radiopharmaceuticals Targeting Integrin alphavbeta6. *ACS Omega*, 2018 3(2): p. 2428–2436. [PubMed: 30023833]
34. Roesch S, et al., Comparative study of the novel RGD motif-containing ITGalphavbeta6 binding peptides SFLAP3 and SFITGv6 for diagnostic application in HNSCC. *J Nucl Med*, 2018.
35. Logan D, et al., Structure of a major immunogenic site on foot-and-mouth-disease virus. *Nature*, 1993 362(6420): p. 566–568. [PubMed: 8385272]
36. Jackson T, et al., The epithelial integrin alphavbeta6 is a receptor for foot-and-mouth disease virus. *J Virol*, 2000 74(11): p. 4949–56. [PubMed: 10799568]
37. Altmann A, et al., Identification of a Novel ITGalphavbeta6-Binding Peptide Using Protein Separation and Phage Display. *Clin Cancer Res*, 2017 23(15): p. 4170–4180. [PubMed: 28468949]
38. Keat N, et al., A Microdose PET Study of the Safety, Immunogenicity, Biodistribution, and Radiation Dosimetry of (18)F-FB-A20FMDV2 for Imaging the Integrin alphavbeta6. *J Nucl Med Technol*, 2018 46(2): p. 136–143. [PubMed: 29438002]
39. Tummers WS, et al., Selection of optimal molecular targets for tumor-specific imaging in pancreatic ductal adenocarcinoma. *Oncotarget*, 2017 8(34): p. 56816–56828. [PubMed: 28915633]

Translational Relevance

The integrin $\alpha_v\beta_6$ is an epithelial-specific cell surface receptor that is undetectable in healthy adult epithelium but significantly up-regulated in a wide range of epithelial-derived cancers. We developed and characterized the [^{18}F] $\alpha_v\beta_6$ -BP PET imaging probe that demonstrated high affinity and selectivity for the integrin $\alpha_v\beta_6$ and was translated into a first-in-human study demonstrating the ability to image both primary and metastatic disease. PET images showed low background uptake in normal brain, lungs, liver and osseous skeleton which are common sites of metastatic disease. Furthermore, sub-centimeter metastasis to these organs from a variety of diverse malignancies including breast, colon, lung and pancreas cancer were detected. The clinical impact of this study is immediate for pre-treatment molecular imaging of a broad spectrum of malignancies; furthermore, this ligand may serve as a cancer-specific delivery platform for the treatment of some of the most lethal malignancies facing patients today.

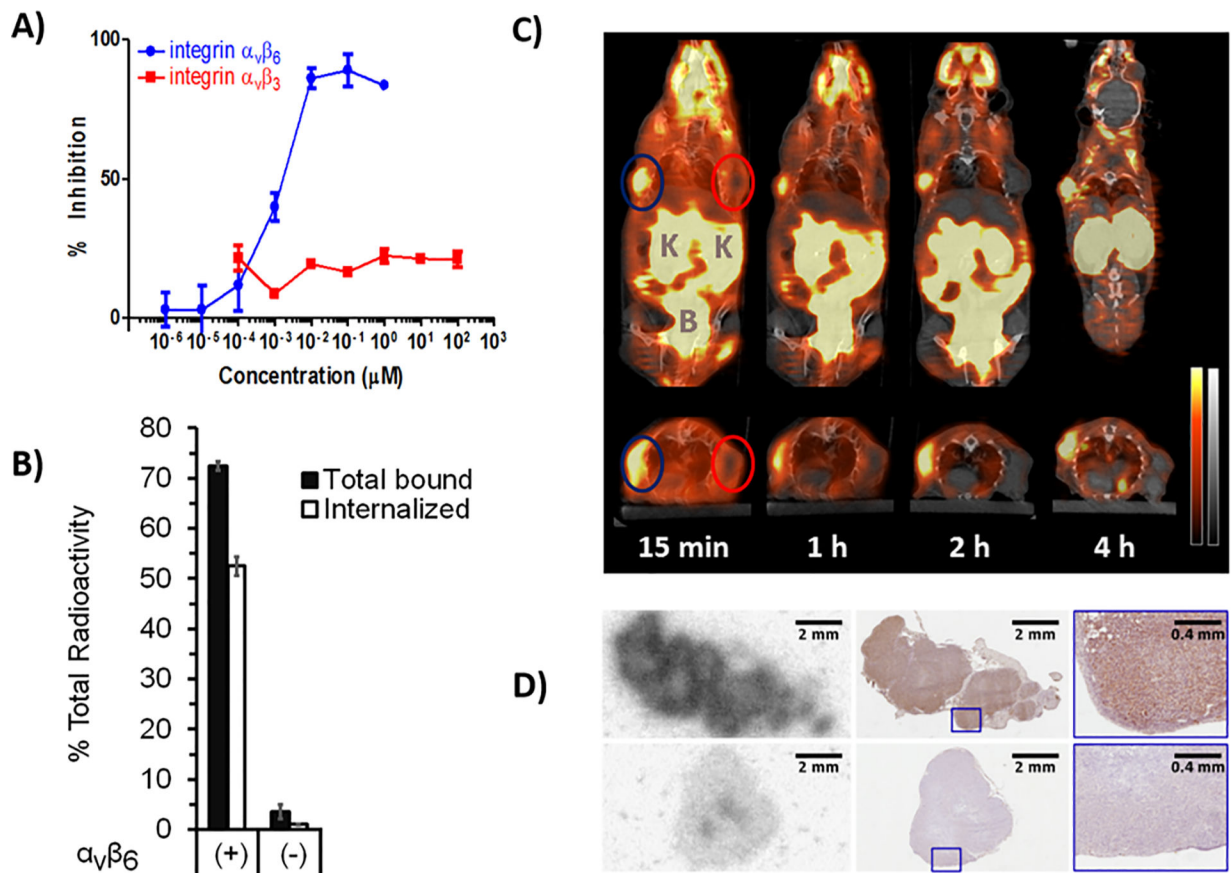


Fig. 1. *In vitro* affinity and selectivity studies and *in vivo* mouse studies with $[\text{}^{18}\text{F}]\alpha_v\beta_6\text{-BP}$. **A)** ELISA binding curves of $[\text{}^{18}\text{F}]\alpha_v\beta_6\text{-BP}$ for integrins $\alpha_v\beta_6$ and $\alpha_v\beta_3$ against biotinylated fibronectin and vitronectin, respectively ($n = 3/\text{integrin}/\text{concentration}$; bars: SD). **B)** Cell-binding and internalization for $[\text{}^{18}\text{F}]\alpha_v\beta_6\text{-BP}$ using the paired integrin $\alpha_v\beta_6$ -expressing DX3puro β_6 cells (+) and $\alpha_v\beta_6$ -null DX3puro control (-). Filled columns: fraction of total radioactivity ($n = 4/\text{cell line}/\text{condition}$; 60 min); bars: SD. **C)** Representative coronal (upper) and transaxial (lower) cross-sections of PET/CT images obtained after injection of $[\text{}^{18}\text{F}]\alpha_v\beta_6\text{-BP}$ (10 MBq) in mouse bearing paired DX3puro β_6 /DX3puro xenografts (112 and 225 mg, blue and red ellipses, respectively). PET: red, CT: gray, K = Kidneys, B = Bladder. **D)** Autoradiography image of DX3puro β_6 (top) and DX3puro (bottom) tumors harvested 1 h after injection of $[\text{}^{18}\text{F}]\alpha_v\beta_6\text{-BP}$ (37 MBq; left) and matched adjacent immunohistochemistry sections stained for integrin $\alpha_v\beta_6$ expression (middle, right; magnified sections).

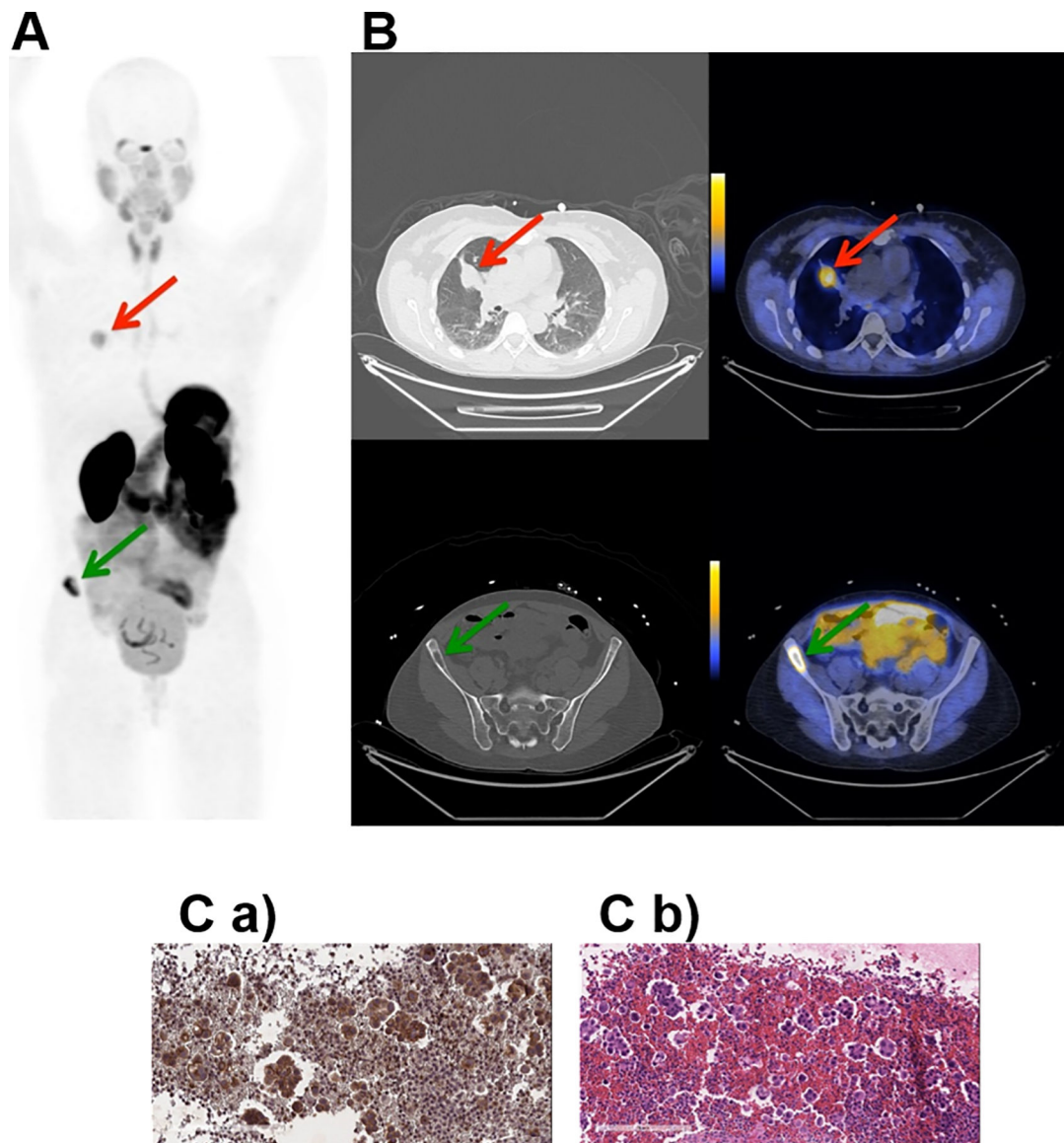


Fig. 2. Representative PET, CT and PET/CT images and IHC staining for subject 1. Subject 1 was a 53 year old female never-smoker with no significant past medical history diagnosed 20 months prior to study enrollment with stage IV adenocarcinoma of the lung. **A.** Coronal maximum intensity projection PET image [scaled to SUV_{max} 15.0] shows distribution of [^{18}F] $\alpha_v\beta_6$ -BP 1 hour after intravenous administration. Red arrow indicates uptake of [^{18}F] $\alpha_v\beta_6$ -BP in primary lung lesion (SUV_{max} 5.2) and green arrow in the Right iliac wing metastasis (SUV_{max} 13.5). **B.** Corresponding axial CT (left) and PET/CT (right) images [scaled to SUV_{max} 7.0] show distribution of [^{18}F] $\alpha_v\beta_6$ -BP in lung mass (top) and right Iliac bone metastasis (bottom). **C. a)** Immunohistochemistry section of sample obtained from pleural fluid (no tissue available for the primary tumor or the right iliac wing metastasis) stained for integrin $\alpha_v\beta_6$ -expression and **b)** corresponding H&E staining.

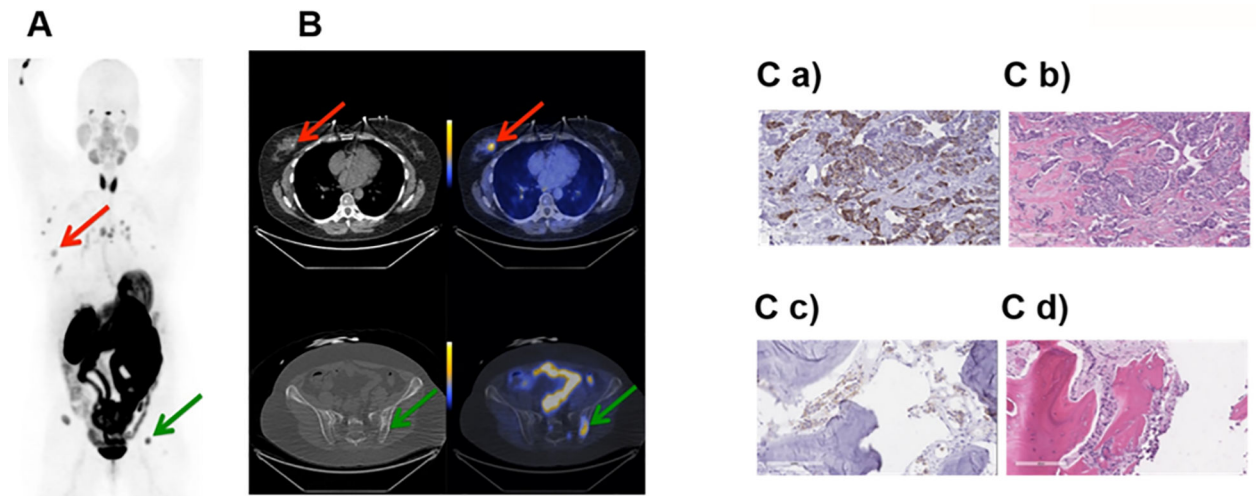


Fig. 3. Representative PET and PET/CT images, and IHC staining for subject 2.

Subject 2 was a 59 year old female diagnosed with Stage IV invasive mammary carcinoma.

A. Coronal maximum intensity projection PET image [scaled to SUV_{max} 15] shows distribution of [^{18}F] $\alpha_v\beta_6$ -BP 1 hour after intravenous administration. Red arrow indicates uptake of [^{18}F] $\alpha_v\beta_6$ -BP in primary breast lesion and green arrow in the left iliac metastasis.

B. Corresponding axial CT (left) and PET/CT (right) images [scaled to SUV_{max} 7] show distribution of [^{18}F] $\alpha_v\beta_6$ -BP in breast mass (SUV_{max} 3.9) and left Iliac bone metastasis (SUV_{max} 13.1). **C.** Immunohistochemistry section stained for integrin $\alpha_v\beta_6$ -expression and corresponding H&E staining of primary breast tumor (a and b) respectively and left Iliac metastasis (c and d) respectively.

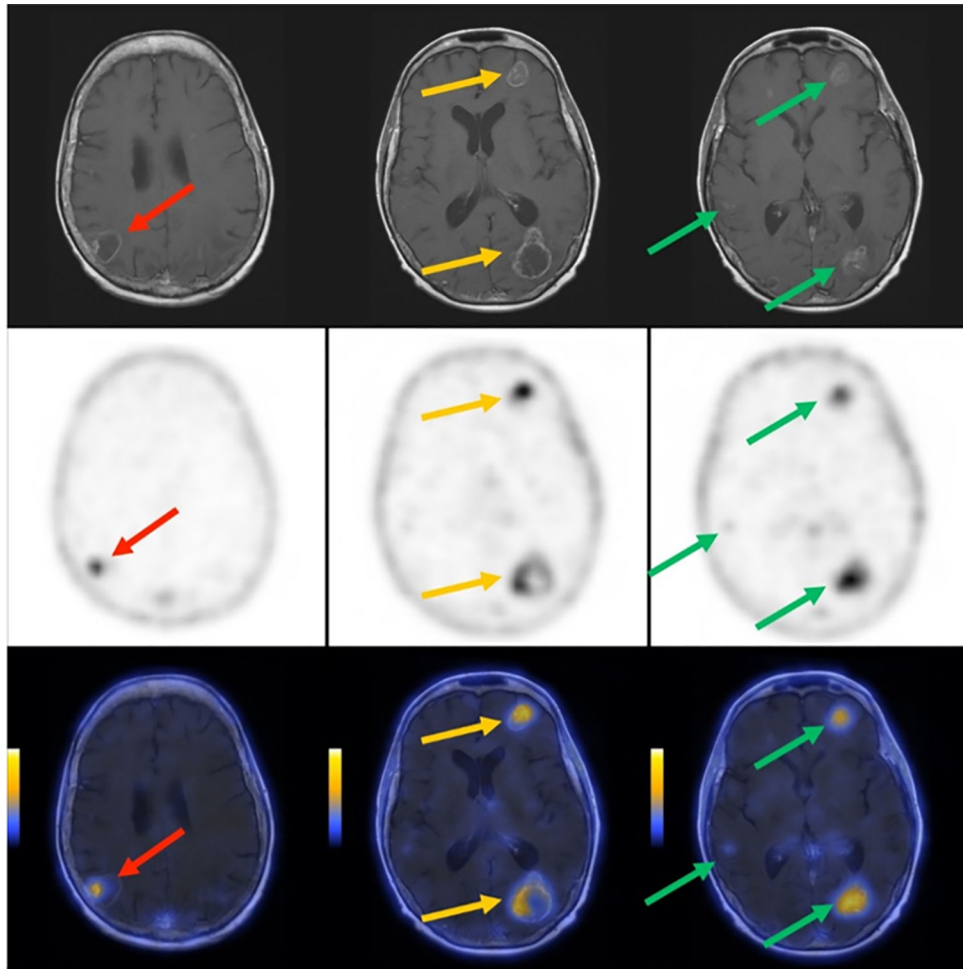


Fig. 4. Representative MRI, PET, and PET/MRI images of brain for subject 3. Subject 3 was a 56 year old female diagnosed with moderately differentiated adenocarcinoma of the lung. Contrast enhanced T1-weighted MRI demonstrating multiple bilateral metastases (upper row). [^{18}F] $\alpha_v\beta_6$ -BP PET images of the brain 1 hour after intravenous administration [^{18}F] $\alpha_v\beta_6$ -BP demonstrating multi-focal elevated activity [scaled to $\text{SUV}_{\text{max}} 2.0$] (middle row). Co-registered fusion images of [^{18}F] $\alpha_v\beta_6$ -BP PET and MRI demonstrating PET activity matched to enhancing lesions [scaled to $\text{SUV}_{\text{max}} 2.0$] (lower row).

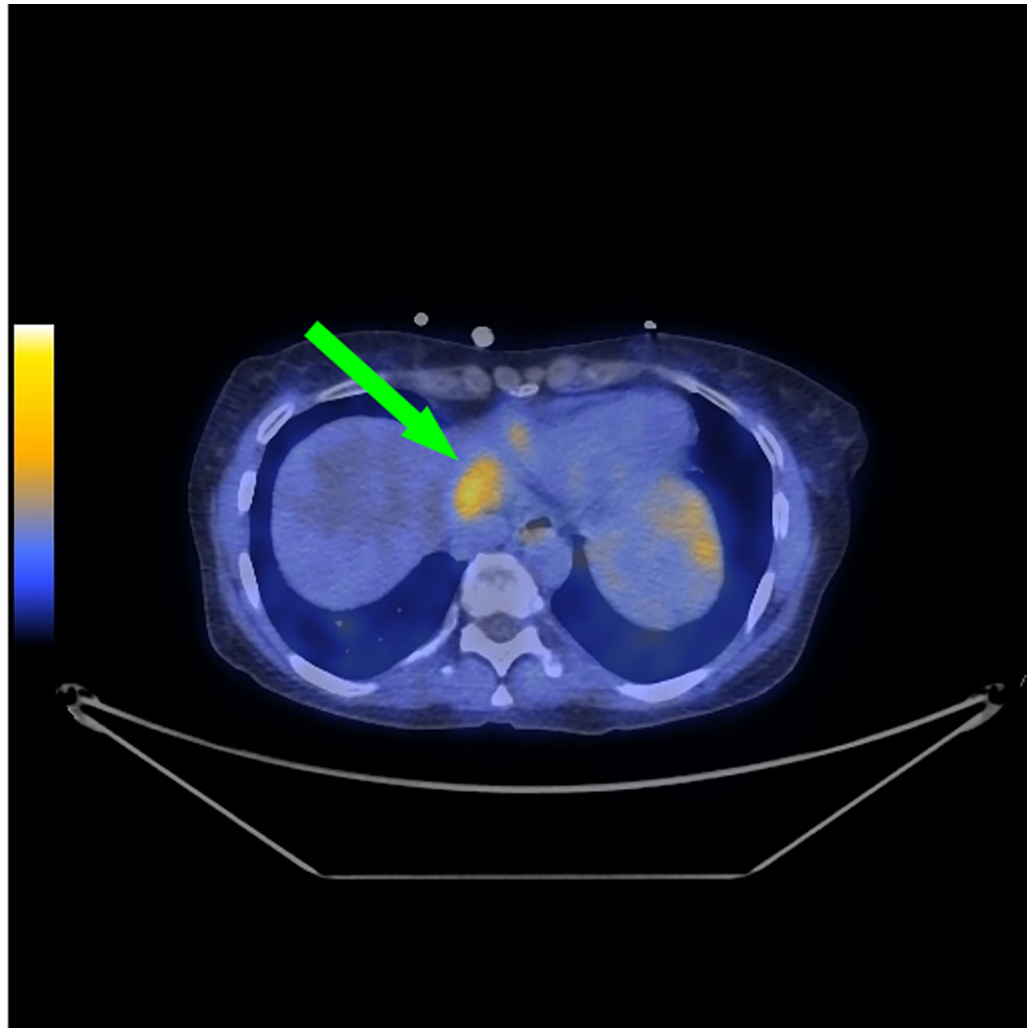


Fig. 5. Representative fused PET/CT for subject 4.

Subject 4 was a 51 year old female diagnosed with initial stage IV adenocarcinoma of the colon with metastases to liver, lungs and abdominal lymph nodes at time of diagnosis. [^{18}F] $\alpha_v\beta_6$ -BP PET/CT images of the upper liver demonstrate elevated activity in the upper left hepatic lobe [scaled to SUV_{max} 3.0] (green arrow).

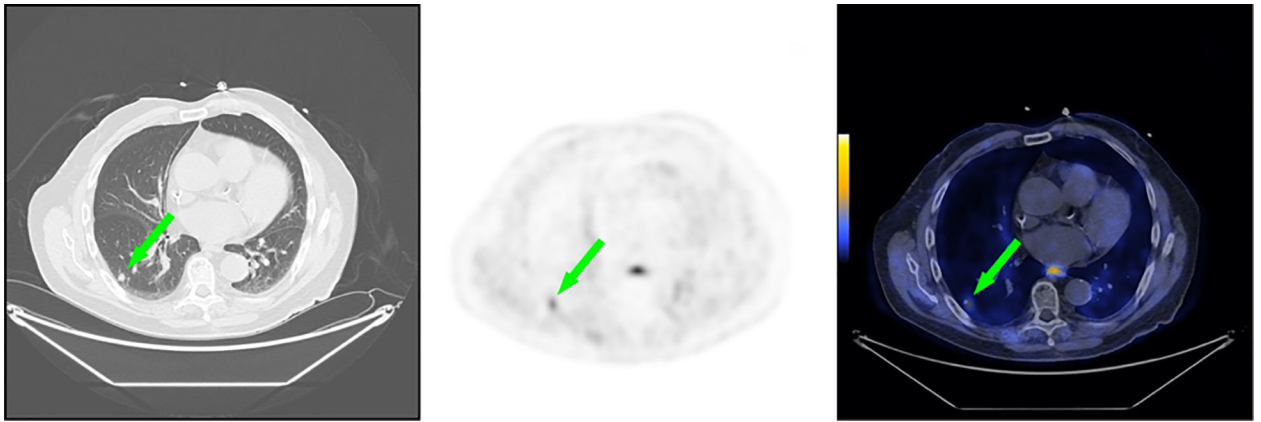


Fig. 6. Representative CT, PET, and fused PET/CT images for subject 5.

Subject 5 was a 78 year old male diagnosed with initial stage IV adenocarcinoma of the pancreas with metastases to the lung at time of diagnosis. Non-contrast CT scan of the chest demonstrates small pulmonary density in the right lower lobe of the lung (left, green arrow). Corresponding [^{18}F] $\alpha_v\beta_6$ -BP PET image of the chest demonstrates elevated activity in the right lower lobe of the lung [scaled to SUV_{max} 5.0] (middle, green arrow). Corresponding [^{18}F] $\alpha_v\beta_6$ -BP fused PET/CT image of the chest demonstrates elevated activity in the right lower lobe of the lung [scaled to SUV_{max} 5.0] (right, green arrow).